

# Caching and Computation Offloading in High Altitude Platform Station (HAPS) Assisted Intelligent Transportation Systems

Qiqi Ren, Omid Abbasi, *Graduate Student Member, IEEE*,

Gunes Karabulut Kurt, *Senior Member, IEEE*,

Halim Yanikomeroglu, *Fellow, IEEE*, and Jian Chen, *Member, IEEE*

## Abstract

Edge intelligence, which is a new paradigm to accelerate artificial intelligence (AI) applications by leveraging computing resources on the network edge, can be used to improve intelligent transportation systems (ITS). However, due to physical limitations and energy-supply constraints, the computing powers of edge equipment are usually limited. High altitude platform station (HAPS) computing can be considered as a promising extension of edge computing. HAPS is deployed in the stratosphere to provide wide coverage and strong computational capabilities. It is suitable to coordinate terrestrial resources and store the fundamental data associated with ITS-based applications. In this work, three computing layers, i.e., vehicles, terrestrial network edges, and HAPS, are integrated to build a computation framework for ITS, where the HAPS data library stores the fundamental data needed for the applications. In addition, the caching technique is introduced for network edges to store some of the fundamental data from the HAPS so that large propagation delays can be reduced. We aim to minimize the delay of the system by optimizing computation offloading and caching decisions as well as bandwidth and computing resource

This work is supported in part by the National Natural Foundation of China (Grant No. 61771366 and Grant No. 61901312), and in part by Huawei Canada.

Q. Ren and J. Chen are with the State Key Laboratory of Integrated Service Networks, Xidian University, Xi' an 710071, Shaanxi, P. R. China, (email: renqiqi5277@gmail.com; jianchen@mail.xidian.edu.cn) (Corresponding Author: Jian Chen).

O. Abbasi and H. Yanikomeroglu are with the Department of Systems and Computer Engineering, Carleton University, Ottawa, ON, Canada (email: {omidabbasi, halim}@sce.carleton.ca).

G. Karabulut Kurt is with the Department of Electrical Engineering, Polytechnique Montréal, Montréal, Canada, e-mail: gunes.kurt@polymtl.ca

allocations. The simulation results highlight the benefits of HAPS computing for mitigating delays and the significance of caching at network edges.

### **Index Terms**

High altitude platform station (HAPS), computation offloading, caching, intelligent transportation systems (ITS).

## **I. INTRODUCTION**

The past decade has witnessed the rapid development of autonomous driving technology, which has mainly been due to progress in deep learning and artificial intelligence (AI) [1]. Autonomous decision-making systems embedded in connected and autonomous vehicles (CAVs) can handle the information generated by vehicular onboard devices, such as cameras, radars, light detection and ranging (LiDAR) sensors, ultrasonic sensors, global positioning systems (GPS), and so on [2] [3]. Through a series of deep learning-based computations, the driving scenario—including path-planning, behavior arbitration, and motion control—can be realized. Generally, deep learning requires massive data to first train a deep neural network (DNN) in a centralized manner, so that the DNN learns to make decisions like humans [4]. After that, the DNN can be deployed or loaded into an application environment. Besides, the application environment also needs to be configured and updated in real time according to the global information of the driving environment. This information, which includes weather conditions, navigations of other CAVs [5], driving conditions of road segments ahead, as well as any emergency CAVs or obstacles to be avoided, can be regarded as fundamental data for the application. The practical application is mainly the process of inference (prediction) of the DNN, which inputs new data encountered in the real world into the pre-trained model yielding results that can guide decision-making [6]. Due to the volume and variety of information, inference processes require relatively complicated computations. In particular, for intelligent transportation systems (ITS) that have huge demands on resources, the design of computing schemes is more demanding and challenging.

Recently, multi-access edge computing (MEC) has been adopted in 5G networks [7]. Compared with centralized cloud computing, MEC provides computation capabilities in proximity, thus improving both delay and energy performance [8], [9]. This makes it possible to push the heavy computational burden of AI to edge computing systems, which has given rise to the research field of edge intelligence (EI) [6]. Thus, by assisting CAVs to perform AI tasks

at edge servers, it has motivated the development of ITS to a certain extent [10]. However, terrestrial edge infrastructures, such as roadside units (RSUs), usually have limited computational capabilities and coverage, making it difficult to provide computation-intensive and sustainable services to CAVs [11]. Much work has been done to find more suitable solutions, for instance, extending edge computing to aerial networks or more remote satellite networks [12]–[17]. Aerial network computing that involves unmanned aerial vehicles (UAVs) can complement terrestrial networks, given that UAVs can be deployed flexibly at relatively low altitudes and offer line-of-sight communications [12]–[14]. However, the small range of coverage as well as the limited battery life and computational capabilities make UAVs unsuitable for long-distance transportation systems. As for satellite networks, recent cutting-edge work has highlighted the potential for strong computational power, but the higher path-loss attenuation leads to larger communication delays, which would be prohibitive for ITS [15]–[17].

More recently, high altitude platform station (HAPS) systems have been proposed as candidates for 6G network [18]–[20]. The HAPS can be adopted as the lead of a stratospheric system operating at an altitude of around 20 km, providing line-of-sight communication and wide coverage with a radius of 50-500 km [21]. It has a large payload (usually  $\geq 100$  kg), which allows to be equipped with powerful computing resources and batteries. In addition, current and future energy conversion techniques for solar energy and wind power as well as battery techniques provide the HAPS with a powerful energy supply potential [22]–[24]. For these reasons, HAPS computing can be viewed as a promising extension of edge computing. The introduction of HAPS computing has three unique advantages for ITS. First, the HAPS can be flexibly deployed and integrated with terrestrial networks to fill the resource shortage, especially for congested and remote areas, without massive updating of terrestrial infrastructures. Second, due to its wide coverage, long battery life as well as the advanced energy conversion technologies, the HAPS can provide more stable and sustainable coverage for ITS, therefore reducing the frequent handoffs between CAVs and terrestrial infrastructures [25]. Finally, the HAPS is suitable for collecting and storing fundamental data, such as the components requested for loading and configuring the ITS-based application environment. Note that since CAVs in the vehicular network may encounter same obstacles, problems, and conditions, HAPS data library is applicable to the entire intelligent transportation network it covers.

It follows from the above that computational performance of CAVs can benefit from the flexible access to the HAPS and RSUs in an integrated system, which means that the tasks of

CAVs that need to be computed can be arranged at three destinations, corresponding to three computational resources: onboard devices of CAVs, terrestrial network edge, and the HAPS. Furthermore, as mentioned above, the HAPS can collect and store fundamental data from a coverage area in its data library. The required fundamental data should be obtained first, and then according to the individual input, a personalized AI inferencing (task computing) can be realized. When computing at a CAV or a network edge is required, the fundamental data needs to be delivered from the HAPS to the computing destination. However, the long-distance transmission of data can cause serious communication delays. To address this issue, this work introduces the caching technique to store frequently requested fundamental data from the HAPS library at the network edge. The cached fundamental data can be accessed more quickly from the edge than from the HAPS, which consequently mitigates delays and improves performance. Considering the dynamic nature of the network and the individual time-varying requirements, we need to reasonably determine the computation offloading policy for each CAV and plan the caching strategy of the fundamental data at network edges as well as to synergistically schedule computing and communication resources to improve delay performance for applications [20], [26], [27]. The main contributions of this work are as follows:

- 1) We introduce HAPS computing for ITS to improve delay performance. To the best of our knowledge, this is the first work that investigates the benefits of the HAPS in accelerating task execution for ITS.
- 2) By integrating the HAPS network with terrestrial edge networks, we develop a three-layer computation framework, in which CAVs can leverage the computing resources of their onboard devices, terrestrial network edges, and the HAPS to deal with the tasks at hand. In addition, by utilizing caching at network edges, we address the issue of large communication delays caused by large-distance transmissions of fundamental data from HAPS.
- 3) With the objective of minimizing the total delay for executing ITS-based tasks, we formulate the optimization problem by considering the computation offloading policy for CAVs and caching strategy of fundamental data at network edges as well as the allocations of computing and bandwidth resources in the network.
- 4) We decouple the formulated mixed-integer nonlinear programming problem (MINP) into decision-making and resource allocation subproblems, where the former addresses compu-

tation offloading and caching decisions, and the latter addresses computing and bandwidth resource allocations. In addition, a multi-agent reinforcement learning method is used to solve the decision-making problem under the assumption of given resource allocations. Then, with the resulting decisions, we determine the optimal resource allocation by using a Lagrangian method.

The remainder of this article is organized as follows. In Section II, we present the system model and the optimization problem formulation. Section III presents a method to solve the decoupled decision-making subproblem. Section IV provides the optimal solution of the decoupled resource allocation subproblem. In Section V, we present the numerical results of the performance evaluation. Finally, Section VI offers some concluding discussions.

## II. SYSTEM MODEL AND OPTIMIZATION FORMULATION

In this section, we present the system model, including the proposed HAPS-assisted caching and computation offloading framework, computing model, caching model, communication model, and delay model, followed by the optimization problem formulation.

### A. Proposed Framework

Fig. 1 shows the proposed HAPS-assisted caching and computation offloading framework for ITS. A single HAPS at an altitude of 20 km in the stratosphere provides coverage for several CAVs along a one-way road [28]. The road is divided into  $M$  segments, labeled as  $\mathcal{M} = \{1, 2, \dots, M\}$ , each of which is covered by an access point, i.e., roadside unit (RSU), and equipped with a server to compute tasks. The CAVs in the objective area are labeled as  $\mathcal{I} = \{1, 2, \dots, I\}$ . In this article, we adopt the quasi-static assumption that the channel environment and network topology remain unchanged in one time slot. Due to the limited computational capabilities of their onboard devices, the CAVs experience serious delays in processing computing-intensive tasks by themselves. Thanks to the proximally situated RSUs and relatively resource-rich HAPS, we can consider a local-RSU-HAPS computation offloading framework for ITS<sup>1</sup>. In this framework, the fundamental data is stored in the HAPS library. The individual data is generated by the onboard devices of CAVs. Note that the fundamental data is

<sup>1</sup>Hereafter, we call computing tasks at the onboard devices of CAVs and RSUs as local computing and RSU computing, respectively.

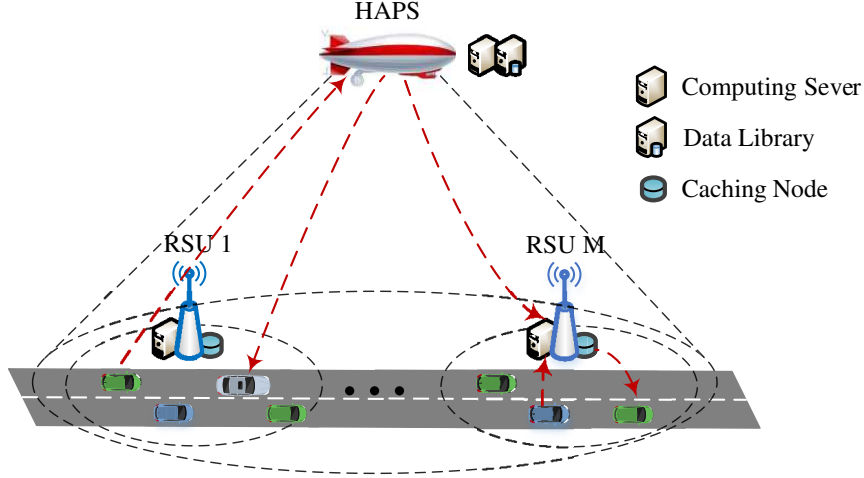


Fig. 1: HAPS-assisted caching and computation offloading framework for ITS.

requested to configure the application environment quickly, and on this basis, personalized tasks can be computed when individual input data is ready. The sequence  $\mathcal{T} = \{1, 2, \dots, T\}$  represents the times of successive decision slots. There are  $N$  fundamental data, which are labeled as the library set  $\mathcal{N} = \{1, 2, \dots, N\}$ . In time slot  $t$ , the volume of the fundamental data requested by CAV  $i$  is represented by  $\Omega_i(t)$ , and the volume of individual data from CAV  $i$  is denoted by  $\varepsilon_i(t)$ . Since the delay performance is critical for ITS, we focus on improving the total delay of all CAVs to complete the tasks. Therefore, the key factors, including the computation offloading decision as well as bandwidth and computing resource allocation will be discussed. Besides, the caching capability of RSUs will also be explored so that the requested fundamental data can be pre-stored for future use to further mitigate delays.

### B. Computing Model

It is assumed that in each time slot  $t$ , each CAV requires only one personalized task computing, which can be executed at only one destination. We use variable  $x_i(t)$  to indicate the computation offloading decision of CAV  $i$ , where  $x_i(t) = 0, 1$ , and  $2$  corresponds to local, HAPS, and RSU computing, respectively. Given offloading decision  $\mathbf{x} = \{x_i(t) | \forall i \in \mathcal{I}\}$ , the CAVs are divided into  $J$  groups according to their computing destinations, including one HAPS computing group,  $M$  RSU computing groups, and one local computing group. The group sets are labeled as  $\Pi = \{\Pi_j | j \in \mathcal{J}\}$ , where  $\mathcal{J} = \{HAPS\} \cup \{RSU_1, RSU_2, \dots, RSU_M\} \cup \{CAV\}$  denotes the index set. As for the computing resources, we first assume that the computational capability for

CAV is  $F_{CAV}$  (in CPU cycle/s). Furthermore, the HAPS and each RSU are equipped with servers with computational capabilities of  $F_{HAPS}$  and  $F_{RSU_m} \forall m \in \mathcal{M}$  (in CPU cycle/s), respectively. We consider that the computing resources are allocated at each RSU and HAPS according to the task workloads, discussed in Section IV. Given this consideration, we let  $f_{i,j}(t)$  indicate the allocated computing resource ratio of CAV  $i$  in computing group  $j$ , and  $\sum_{i \in \Pi_j} f_{i,j}(t) \leq 1, \forall j \in \{\mathcal{J} \setminus CAV\}$  limit the computing resource allocation at each server. Furthermore, the computation delay can be expressed as  $\frac{\lambda_i(t)}{f_{i,j}(t)F_j}$  for  $\forall j \in \{\mathcal{J} \setminus CAV\}$ , and  $\frac{\lambda_i(t)}{F_{CAV}}$  for  $j = CAV$ , where  $\lambda_i(t)$  is the required workloads for processing CAV  $i$ 's task, obtained by the product of individual input data  $\varepsilon_i(t)$  (in bit) and computation density  $e_i(t)$  (in CPU cycle/bit).

### C. Caching Model

Each RSU is equipped with storage, whose space is  $C$  (in Mbits). The requested fundamental data, which is not in the storage, can be cached for future reuse. The storage follows the first-in-first-out policy, which means that when the content needs to be updated and the space is insufficient, the most previously stored content will be deleted [26]. We let binary variable  $y_i(t)$  to indicate the decision of whether to cache the fundamental data requested by CAV  $i$  at the end of time slot  $t$ , where  $y_i(t) = 1$  means it will be cached at CAV  $i$ 's associated RSU, while  $y_i(t) = 0$  means it will not be cached. Let binary variable  $s_i(t)$  indicate the state of whether CAV  $i$ 's requested fundamental data is in the storage of its associated RSU, where  $s_i(t) = 1$  means it is in the storage, while  $s_i(t) = 0$  means it is not. When the task is performed by CAV  $i$  or its associated RSU, it can receive a fast response if the requested fundamental data is in storage; otherwise, it will get the content from the HAPS library.

### D. Communication Model

We consider both RSUs and CAVs are equipped with a single antenna, while the HAPS is equipped with multiple antennas, and the objective area represents one HAPS cell. Meanwhile, all links between the HAPS and CAVs, between the HAPS and RSUs, and between RSUs and CAVs work on orthogonal channels. Fig. 2 shows all links in the communication system. Link ① is the downlink from the HAPS to the RSU for transmitting fundamental data; Link ② is the downlink from the HAPS to CAV  $i$  for transmitting fundamental data or the computed result; Link ③ is the uplink from CAV  $i$  to HAPS for offloading individual input data; Link ④ is the downlink from the RSU to CAV  $i$  for transmitting fundamental data or the computed result;



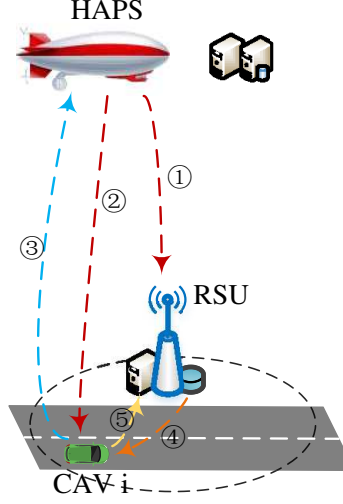


Fig. 2: Communication model.

Link ⑤ is the uplink from CAV  $i$  to the RSU for offloading individual input data. Since the HAPS hovers in the stratosphere, we consider line-of-sight (LoS) links for links ①, ② and ③, whose large-scale fading path loss follows the free space path loss, and the overall channel gain can be modeled by [29]:

$$G_i^{LoS}(t) = G \left( \frac{c}{4\pi d_i(t) f_c} \right)^2 |h_i^{LoS}(t)|^2 \quad i \in \mathcal{I} \quad (1)$$

where  $c$  is the speed of light,  $d_i(t)$  is the distance of the link from the transmitter to receiver.  $f_c$  is the carrier frequency, and we consider 2 GHz for all links in this work.  $G$  is the directional antenna gain corresponding to the production of the transmitter antenna gain and receiver antenna gain. Since environment effects are negligible for the frequencies under 10 GHz, the environment attenuations are not considered in this work [30].  $h_i^{LoS}(t)$  is the small-scale fading coefficient of the LoS links, corresponding to Rice fading.

Links ④ and ⑤ are non-line-of-sight (NLoS) communication links, whose channel gains are modeled as follows:

$$G_i^{NLoS}(t) = \frac{\beta_0(f_c) |h_i^{NLoS}(t)|^2}{(d_i(t))^\alpha} \quad (2)$$

where  $\beta_0(f_c)$  is the path loss at the reference distance 1 m,  $h_i^{NLoS}(t)$  is the small-scale fading coefficient of the NLoS links following a Rayleigh distribution, and  $\alpha$  is the path-loss exponent.

To improve the delay performance, bandwidth resources are allocated among links on the basis of channel gain and the volume of the transmitted data in this work, discussed in Section



IV. In order to discuss the bandwidth allocation, we categorize all CAVs in the communication system into four groups, according to offloading decision  $\mathbf{x}$  and caching state  $\mathbf{s}$  of the requested fundamental data. The group sets of CAVs are labeled as  $\Psi = \{\Psi_k | k \in \mathcal{K}\}$ , where  $\mathcal{K} = \{dl\_H, ul\_H, dl\_R, ul\_R\}$  is the index set of groups. By discussing the situation of CAV  $i$ , the group specifications and forming standards are listed as follows:

- 1)  $dl\_H$ : The downlink transmission of the HAPS, including links ① and ②. For CAV  $i$ , link ① corresponds to  $x_i(t) = 2, s_i(t) = 0$ , where fundamental data needs to be transmitted from the HAPS to CAV  $i$ 's associated RSU. Link ② corresponds to  $x_i(t) = 0, s_i(t) = 0$  or  $x_i(t) = 1$ , where the fundamental data or computed result will be transmitted from the HAPS to CAV  $i$ . The available bandwidth of CAVs in group  $k = dl\_H$  is  $B_{dl\_H}$ .
- 2)  $ul\_H$ : The uplink transmission of the HAPS, corresponding to link ③ with the offloading decision  $x_i(t) = 1$ , where the individual input data will be transmitted from CAV  $i$  to the HAPS. The available bandwidth of CAVs in group  $k = ul\_H$  is  $B_{ul\_H}$ .
- 3)  $dl\_R$ : The downlink transmission of an RSU, corresponding to link ④ with  $x_i(t) = 0, s_i(t) = 1$  or  $x_i(t) = 2$ , where the fundamental data or the computed results will be transmitted from the associated RSU to CAV  $i$ . The available bandwidth of CAVs in group  $k = dl\_R$  is  $B_{dl\_R}$ .
- 4)  $ul\_R$ : The uplink transmission of the RSU, corresponding to link ⑤ with  $x_i(t) = 2$ , where the individual input data will be transmitted from CAV  $i$  to its associated RSU. The available bandwidth of CAVs in group  $k = ul\_R$  is  $B_{ul\_R}$ .

Based on the above categorization, the channel gains can be restated as  $G_{i,k}(t), \forall i \in \Psi_k, \forall k \in \mathcal{K}$ , in which each composition is from the channel gain given at either equation (1) or equation (2). Therefore, the transmission rate can be given accordingly:

$$R_{i,k}(t) = b_{i,k}(t)B_k \log_2 \left( 1 + \frac{P_k^T G_{i,k}(t)}{b_{i,k}(t)B_k N_0} \right) \quad (3)$$

where  $b_{i,k}(t)$  is the ratio of bandwidth allocated to CAV  $i$  in group  $k$ , and  $\sum_{i \in \Psi_k} b_{i,k}(t) \leq 1, \forall k \in \mathcal{K}$  constrains the bandwidth ratios of the CAVs belonging to each group.  $B_k$  is the available bandwidth of CAV  $i$  in group  $k$ , and  $N_0$  is the Gaussian noise power spectrum density. With the transmission rate, the communication delay can be modeled as  $\frac{D_i(t)}{R_{i,k}(t)}$  for CAV  $i$  in group  $k$ , where  $D_i(t)$  represents the volume of data to be transmitted, which includes fundamental data  $\Omega_i(t)$ , individual input data  $\varepsilon_i(t)$ , and the computed result (output data)  $\varphi_i(t)$ .

### E. Delay Model

Thus far, the computing, caching, and communication models have been formulated. Using these models, the delays of CAV  $i$  under computing ways of local, HAPS, and RSU are given as follows:

#### 1) Local computing

$$T_i^L(t) = \mathbb{1}_{x_i(t)=0} \cdot \left( \frac{s_i(t)\Omega_i(t)}{R_{i,dl\_R}(t)} + \frac{(1-s_i(t))\Omega_i(t)}{R_{i,dl\_H}(t)} + \frac{\lambda_i(t)}{F_{CAV}} \right) \quad (4)$$

#### 2) HAPS computing

$$T_i^H(t) = \mathbb{1}_{x_i(t)=1} \cdot \left( \frac{\varepsilon_i(t)}{R_{i,ul\_H}(t)} + \frac{\lambda_i(t)}{f_{i,HAPS}(t)F_{HAPS}} + \frac{\varphi_i(t)}{R_{i,dl\_H}(t)} \right) \quad (5)$$

#### 3) RSU computing

$$T_i^R(t) = \mathbb{1}_{x_i(t)=2} \cdot \left( \frac{(1-s_i(t))\Omega_i(t)}{R_{i,dl\_H}(t)} + \frac{\varepsilon_i(t)}{R_{i,ul\_R}(t)} + \frac{\lambda_i(t)}{f_{i,RSU_m}(t)F_{RSU_m}|_{i \in \Pi_{RSU_m}}} + \frac{\varphi_i(t)}{R_{i,dl\_R}(t)} \right) \quad (6)$$

where  $\mathbb{1}_\Theta$  is a conditional indicator which equals 1 when condition  $\Theta$  is true; otherwise it equals 0.

### F. Optimization Problem Formulation

Here, we formulate an optimization that optimizes the computation offloading decision  $\mathbf{x}$ , caching decision  $\mathbf{y}$ , bandwidth resource allocation  $\mathbf{b}$ , and computing resource allocation  $\mathbf{f}$  for all CAVs, with the objective of minimizing the delays experienced by CAVs for executing tasks over multiple time slots. The optimization details are mathematically formulated as follows:

$$\min_{\mathbf{x}, \mathbf{y}, \mathbf{b}, \mathbf{f}} \sum_{t \in \mathcal{T}} \sum_{i \in \mathcal{I}} T_i^L(t) + T_i^R(t) + T_i^H(t) \quad (7a)$$

$$x_i(t) \in \{0, 1, 2\} \quad \forall i \in \mathcal{I}, \forall t \in \mathcal{T} \quad (7b)$$

$$y_i(t) \in \{0, 1\} \quad \forall i \in \mathcal{I}, \forall t \in \mathcal{T} \quad (7c)$$

$$\sum_{i \in \Psi_k} b_{i,k}(t) \leq 1 \quad \forall k \in \mathcal{K}, \forall t \in \mathcal{T} \quad (7d)$$

$$\sum_{i \in \Pi_j} f_{i,j}(t) \leq 1 \quad \forall j \in \mathcal{J}, \forall t \in \mathcal{T} \quad (7e)$$

$$b_{i,k}(t) > 0 \quad \forall i \in \Psi_k, \forall k \in \mathcal{K}, \forall t \in \mathcal{T} \quad (7f)$$

$$f_{i,j}(t) > 0 \quad \forall i \in \Pi_j, \forall j \in \{\mathcal{J} \setminus CAV\}, \forall t \in \mathcal{T} \quad (7g)$$

where (7a) is the optimization objective function of the total delay of all CAVs over several time slots, which consists of the delays under three ways: local, RSU, and HAPS computing. (7b)

indicates the offloading decision of CAVs for executing tasks, and (7c) indicates the caching decision of the requested fundamental data of CAVs. (7d) denotes the bandwidth constraints for different types of links. (7e) denotes the computing resource constraints of the HAPS and RSUs. (7f) and (7g) are positive requirements for resource allocation variables.

Problem (7) is a mixed-integer nonlinear programming (MINP) problem with coupled computation offloading and caching decisions as well as bandwidth and computing variables, which is NP-hard to solve. In the following, we decouple the optimization problem into two subproblems, where we first adopt the multi-agent reinforcement learning method to solve the decision-making problem over several time slots. Then, with the given decisions, we find the efficient solutions of the bandwidth and computing resource allocations in each time slot.

### III. THE MARL-BASED DECISION-MAKING PROBLEM FOR COMPUTATION OFFLOADING AND CACHING

We first discuss the decision-making problem for computation offloading and caching decisions, by adopting equal communication and computing resource allocations. The decision-making optimization problem is given as follows:

$$\min_{\mathbf{x}, \mathbf{y}} \sum_{t \in \mathcal{T}} \sum_{i \in \mathcal{I}} T_i^L(t) + T_i^R(t) + T_i^H(t) \quad (8a)$$

$$x_i(t) \in \{0, 1, 2\} \quad \forall i \in \mathcal{I}, \forall t \in \mathcal{T} \quad (8b)$$

$$y_i(t) \in \{0, 1\} \quad \forall i \in \mathcal{I}, \forall t \in \mathcal{T}. \quad (8c)$$

This allows us to determine the computation offloading and caching over multiple time slots. We will use a multi-agent deep reinforcement (MARL) learning method to solve this problem, where each CAV represents an agent making the offloading and caching decisions. Multi-agent systems (MAS) have been used in a wide range of fields, including telecommunications, distributed control, resource management, and collaborative decision support systems [31]. Reinforcement learning (RL) can help solve multi-agent problems over multiple time slots by enabling agents to interact sequentially with the environment, take actions, and perceive states and rewards to maximize cumulative rewards [32]. Depending on the relationship between the agents, MARL can be divided into three types: cooperative, competitive, and mixed. In this article, we consider the proposed architecture as a cooperative MARL problem where agents are independent decision-makers who coordinate their actions and work together to achieve a shared team reward accumulated over time [31].

### A. Dec-POMDP

The training process of this MARL is modeled as a decentralized partially observable Markov decision process (Dec-POMDP), whose main components are defined as follows:

- 1) Actions: At each time slot  $t$ , each agent  $i \in I$  chooses an action  $u_i(t) \in \mathcal{U}$ , forming a joint action  $\mathbf{u}_t \in \mathcal{U}$ . In this article, each agent  $i$  needs to make offloading and caching decisions, and therefore the action space of  $\mathcal{U}$  derives from combinations of  $x_i(t) = 0, 1$ , or 2 and  $y_i(t) = 0$  or 1. Note that when agent  $i$  chooses either local computing or HAPS computing, we do not need to consider whether to cache the requested fundamental data at the RSU; therefore, the action space  $\mathcal{U}$  can be defined as four elements for each agent. Here, we define  $u_i(t) = 0$ , and 1 to represent agent  $i$  choosing local computing and HAPS computing for its task, respectively. And we define  $u_i(t) = 2$  for the case that the agent  $i$  chooses RSU computing for its task and the requested fundamental data will not be cached at the associated RSU at the end of the time slot  $t$ .  $u_i(t) = 3$  means that agent  $i$  will choose RSU computing and the requested fundamental data will be cached.
- 2) Observations:  $o_i(t)$  is the observation of agent  $i$ , and  $\mathbf{o}_t$  is a joint observation. Here we regard the joint observation  $\mathbf{o}_t$  as the global state of the whole system. Each agent perceives its own observation independently without communicating with others. This assumption is due to the difficulty of communicating with running CAVs and the limited sensing capabilities of onboard devices. The observation space includes the following:
  - a) The channel gains of uplink and downlink of HAPS transmissions, i.e.,  $G_{i,ul\_H}(t)$ ,  $G_{i,dl\_H}(t)$ , as well as uplink and downlink of RSU transmissions, i.e.,  $G_{i,ul\_R}(t)$ ,  $G_{i,dl\_R}(t)$ .
  - b) The individual input data volume  $\varepsilon_i(t)$ , the output data volume  $\varphi_i(t)$ , and the computation density  $e_i(t)$ .
  - c) The index of the requested fundamental data  $n_i(t)$ , and the flag  $s_i(t)$  indicating whether the requested content of agent  $i$  is stored with its associated RSU.
- 3) Team reward: In this system, each agent receives the joint team reward despite their individual observations and separate actions. Considering the objective is to reduce the total delay of CAVs, we use the sigmoid function to normalize the negative value of the total delay as the reward value  $r_t$ .

With these definitions, the sequential decision-making optimization problem in a dynamic

environment can be formulated as a Dec-POMDP. The goal of all agents is to maximize the expected cumulative discounted joint reward, i.e.,  $\mathcal{R}_t = \sum_{m=0}^{\infty} \gamma^m r_{t+m}$ , where  $\gamma$  is the discount factor.

### B. Solving the Problem with Value-Decomposition Networks

One commonly used method in MAS is the independent Q-learning (IQL) algorithm, which decomposes the multi-agent problem into a set of simultaneous single-agent problems in a shared environment with multiple agents [33]. The partial observability of each agent is such that they are unable to observe the global state of the environment. More concretely, under the same observation  $o_i(t)$ , although agent  $i$  can take the same action, the joint team reward obtained may be different, because the global state may be different, and the policies of other agents are always changing, which leads to instability across the whole system. We adopt a centralized training decentralized execution (CTDE) framework in the collaborative MAS, which allows the global state to be acquired during the centralized training, and the agents can make independent decisions based on local observations only. However, a joint action-value function  $Q_{tot}(\mathbf{o}_t, \mathbf{u}_t)$  obtained during the centralized training will not be exploited during distributed execution as only local observations can be acquired. A new proposal of value decomposition networks (VDNs) can be applied during the training process to decompose  $Q_{tot}(\mathbf{o}_t, \mathbf{u}_t)$  into individual action-value functions  $Q_i(o_i(t), u_i(t)), \forall i \in \mathcal{I}$ . This is an enhancement that builds on the deep Q-learning network (DQN) to overcome the issue mentioned above [33]. The VDN algorithm learns a joint action-value function  $Q_{tot}(\boldsymbol{\tau}_t, \mathbf{u}_t)$ , where  $\boldsymbol{\tau}_t$  is a joint action-observation history (replacing the global state  $\mathbf{o}_t$  in partially observable system) with each component defined as  $\tau_i(t) = u_i(1)o_i(1)r_1, \dots, u_i(t-1)o_i(t-1)r_{t-1}$ .  $Q_{tot}(\boldsymbol{\tau}_t, \mathbf{u}_t)$  is approximately the sum of all independent action-value functions  $Q_i(o_i(t), u_i(t))$  which is only relevant to individual action-observation history, i.e.,

$$Q_{tot}(\boldsymbol{\tau}_t, \mathbf{u}_t) \approx \sum_i^I Q_i(\tau_i(t), u_i(t); \theta_i(t)) \quad (9)$$

where  $\theta$  is the parameter of the network as in DQN. Building on DQN, the VDN algorithm adopts the fixed target network and an experience replay buffer, and it utilizes the joint reward to iteratively update network parameters to minimize the following loss function:

$$L(\theta) = \mathbb{E} \left[ \left( y^{tot} - Q_{tot}(\boldsymbol{\tau}_t, \mathbf{u}_t) \right)^2 \right]. \quad (10)$$

This expectation is over the mini-batches drawn from the experience replay buffer. The target value is defined by  $y^{tot} = r_t + \gamma \max_{u_{t+1}} Q_{tot}(\tau_{t+1}, \mathbf{u}_{t+1})$ . The gradients are backpropagated following the Q-learning rule to update  $Q_i$  for each agent  $i$ . As a result, the VDN algorithm allows the use of global information during the centralized training and enables agents to execute actions independently according to local observations.

#### IV. OPTIMAL ALLOCATION FOR BANDWIDTH AND COMPUTING RESOURCES

In this section, we investigate the optimal bandwidth and computing resource allocation problem in (7) with the given computation offloading policy and caching strategy. Concretely, we utilize the Lagrangian dual method to formulate the Karush-Kuhn-Tucker (KKT) conditions of the problem, and then we find the closed-form solution for bandwidth resource allocation, and the optimal solution for computing resource allocation by using a bisection search method.

Since the resource allocation problem is developed within one time slot, for brevity, we omit “( $t$ )” below, e.g.,  $f_{i,j}$  will represent  $f_{i,j}(t)$ , unless the time slot  $t$  is emphasized. Assuming the computation offloading and caching decisions are given, we first rewrite the resource allocation problem as follows:

$$\begin{aligned} \min_{\mathbf{b}, \mathbf{f}} \quad & \sum_{k \in \mathcal{K}} \sum_{i \in \Psi_k} \frac{O_{i,k}}{b_{i,k} \log_2(1 + \frac{H_{i,k}}{b_{i,k}})} + \sum_{j \in \{\mathcal{J} \setminus CAV\}} \sum_{i \in \Pi_j} \frac{U_{i,j}}{f_{i,j}} \\ & + \sum_{i \in \Pi_{CAV}} \frac{\lambda_i}{F_{CAV}} \end{aligned} \quad (11a)$$

$$\sum_{i \in \Psi_k} b_{i,k} \leq 1 \quad \forall k \in \mathcal{K} \quad (11b)$$

$$\sum_{i \in \Pi_j} f_{i,j} \leq 1 \quad \forall j \in \{\mathcal{J} \setminus CAV\} \quad (11c)$$

$$b_{i,k} > 0 \quad \forall i \in \Psi_k, \forall k \in \mathcal{K} \quad (11d)$$

$$f_{i,j} > 0 \quad \forall i \in \Pi_j, \forall j \in \{\mathcal{J} \setminus CAV\}. \quad (11e)$$

In (11a), the first term denotes the communication delays, where  $O_{i,k} = \frac{D_i}{B_k}$  and  $H_{i,k} = \frac{P_k^T G_{i,k}}{B_k N_0}$ . The second term denotes the computation delays at the servers, where  $U_{i,j} = \frac{\lambda_i}{F_j}$ . The third term denotes the computation delays at the CAVs, which can be omitted in the further analysis of the problem (11) since the available computational capabilities of the CAVs are fixed in this work. (11b) to (11e) are constraints of bandwidth and computing resource allocations.

**Proposition 1:** Problem (11) is convex.

*Proof.* For simplicity, we first define functions  $w(b_{i,k}) = b_{i,k} \log_2 \left(1 + \frac{H_{i,k}}{b_{i,k}}\right)$ ,  $g(b_{i,k}) = \frac{O_{i,k}}{w(b_{i,k})}$ , and  $z(f_{i,j}) = \frac{U_{i,j}}{f_{i,j}}$ . As a consequence, the second-order derivatives can be calculated as

$$w''(b_{i,k}) = -\frac{H_{i,k}^2}{\ln 2 \times b_{i,k}(b_{i,k} + H_{i,k})^2} \quad (12)$$

$$g''(b_{i,k}) = \frac{O_{i,k} \left[ 2(w'(b_{i,k}))^2 - w''(b_{i,k})w(b_{i,k}) \right]}{w^3(b_{i,k})} \quad (13)$$

and

$$z''(f_{i,j}) = \frac{2U_{i,j}}{f_{i,j}^3}. \quad (14)$$

From (12), we can observe that  $w''(b_{i,k}) < 0$ , and therefore  $g''(b_{i,k}) > 0$  holds and the convexity of  $g(b_{i,k})$  can be obtained. From (14), we can obtain the convexity of  $z(f_{i,j})$  and the proof is completed.  $\square$

Since problem (11) is a standard convex optimization problem, we can solve it by using general convex optimization methods such as the interior point method. However, the complexity of the interior point method increases quickly with the number of CAVs. Now we will use Lagrangian dual method to find the solution efficiently. Let us introduce the Lagrangian multipliers for constraints (11b) and (11c) to formulate a partial Lagrangian function:

$$\mathcal{L}(\mathbf{b}, \mathbf{f}, \boldsymbol{\eta}, \boldsymbol{\mu}) = \sum_{k \in \mathcal{K}} \sum_{i \in \Psi_k} g(b_{i,k}) + \sum_{j \in \{\mathcal{J} \setminus CAV\}} \sum_{i \in \Pi_j} z(f_{i,j}) + \sum_{k \in \mathcal{K}} \eta_k \left( \sum_{i \in \Psi_k} b_{i,k} - 1 \right) + \sum_{j \in \{\mathcal{J} \setminus CAV\}} \mu_j \left( \sum_{i \in \Pi_j} f_{i,j} - 1 \right). \quad (15)$$

Following this, the Lagrangian dual function is given by

$$\mathcal{D}(\boldsymbol{\eta}, \boldsymbol{\mu}) = \min_{\mathbf{b}, \mathbf{f}} \{ \mathcal{L}(\mathbf{b}, \mathbf{f}, \boldsymbol{\eta}, \boldsymbol{\mu}) \mid \mathbf{b} > \mathbf{0}, \mathbf{f} > \mathbf{0} \} \quad (16)$$

and the dual problem is

$$\max_{\boldsymbol{\eta}, \boldsymbol{\mu}} \{ \mathcal{D}(\boldsymbol{\eta}, \boldsymbol{\mu}) \mid \boldsymbol{\eta} \geq \mathbf{0}, \boldsymbol{\mu} \geq \mathbf{0} \}. \quad (17)$$

As (11) is a convex problem, the dual problem can achieve the same optimal objective with the primal problem by the strong duality [34]. In the following, we provide the analysis of the KKT conditions of (11), which are sufficient and necessary for the optimal solution and yield a computationally efficient algorithm. The KKT conditions are expressed as follows:

$$\nabla_{b_{i,k}} \mathcal{L}(\mathbf{b}, \mathbf{f}, \boldsymbol{\eta}, \boldsymbol{\mu}) = 0 \quad \forall i \in \Psi_k, \forall k \in \mathcal{K} \quad (18a)$$

$$\nabla_{f_{i,j}} \mathcal{L}(\mathbf{b}, \mathbf{f}, \boldsymbol{\eta}, \boldsymbol{\mu}) = 0 \quad \forall i \in \Pi_j, \forall j \in \{\mathcal{J} \setminus CAV\} \quad (18b)$$

$$\eta_k \left( \sum_{i \in \Psi_k} b_{i,k} - 1 \right) = 0 \quad \forall k \in \mathcal{K} \quad (18c)$$



$$\mu_j \left( \sum_{i \in \Pi_j} f_{i,j} - 1 \right) = 0 \quad \forall j \in \{\mathcal{J} \setminus CAV\} \quad (18d)$$

$$\sum_{i \in \Psi_k} b_{i,k} - 1 \leq 0 \quad \forall k \in \mathcal{K} \quad (18e)$$

$$\sum_{i \in \Pi_j} f_{i,j} - 1 \leq 0 \quad \forall j \in \{\mathcal{J} \setminus CAV\} \quad (18f)$$

$$b_{i,k} > 0 \quad \forall i \in \Psi_k, \forall k \in \mathcal{K} \quad (18g)$$

$$f_{i,j} > 0 \quad \forall i \in \Pi_j, \forall j \in \{\mathcal{J} \setminus CAV\} \quad (18h)$$

$$\eta_k \geq 0 \quad \forall k \in \mathcal{K} \quad (18i)$$

$$\mu_j \geq 0 \quad \forall j \in \{\mathcal{J} \setminus CAV\}. \quad (18j)$$

Here, (18a) and (18b) are necessary conditions for the feasible solution of the Lagrangian function; (18c) and (18d) are relaxation complementary conditions; (18e) to (18h) are primal constraints; (18i) and (18j) are the conditions that should be met for the Lagrangian multipliers of inequality constraints.

We use the definitions of  $g(b_{i,k}) = \frac{O_{i,k}}{b_{i,k} \log_2(1 + \frac{H_{i,k}}{b_{i,k}})}$  and  $z(f_{i,j}) = \frac{U_{i,j}}{f_{i,j}}$  to make further discussions. According to (18a) and (15), we can obtain that

$$g'(b_{i,k}) + \eta_k = 0 \quad \forall i \in \Psi_k, \forall k \in \mathcal{K}. \quad (19)$$

**Proposition 2:** The root  $\eta_k^*$  of (19) is unique and positive.

*Proof.* Recalling (13) in the Proof of Proposition 1,  $g''(b_{i,k}) > 0$ , which indicates the first-order derivative of  $g(b_{i,k})$  is a monotonically increasing function, calculated as follows:

$$g'(b_{i,k}) = - \frac{\ln 2 \times O_{i,j} \left( (b_{i,j} + H_{i,j}) \ln \left( 1 + \frac{H_{i,j}}{b_{i,j}} \right) - H_{i,j} \right)}{b_{i,j}^2 (b_{i,j} + H_{i,j}) \ln^2 \left( 1 + \frac{H_{i,j}}{b_{i,j}} \right)}. \quad (20)$$

Therefore, we can obtain  $g'(b_{i,k}) \leq g'(1)$ . In order to determine  $g'(b_{i,k})$ , we need to discuss  $g'(1)$ , which is expressed by  $g'(1) = - \frac{\ln 2 \times O_{i,j} ((1+H_{i,j}) \ln(1+H_{i,j}) - H_{i,j})}{(1+H_{i,j}) \ln^2(1+H_{i,j})}$ . It is difficult to observe whether  $g'(1)$  is a negative or a positive value directly. Now, we further let  $\mathcal{Z}(H_{i,j}) = (1 + H_{i,j}) \ln(1 + H_{i,j}) - H_{i,j}$ . The first-order derivative of  $\mathcal{Z}(H_{i,k})$  is calculated as  $\mathcal{Z}'(H_{i,k}) = \ln(1 + H_{i,k})$ . It is clear that  $\mathcal{Z}'(H_{i,k}) > 0$ , which indicates function  $\mathcal{Z}(H_{i,k})$  monotonously increases with  $H_{i,k}$ . Consequently,  $\mathcal{Z}(H_{i,k}) > \mathcal{Z}(0) = 0$  (Note that  $H_{i,k} > 0$ ). After that, we can obtain  $g'(1) < 0$ . And accordingly  $g'(b_{i,k}) < 0$  holds, where  $b_{i,k} \in (0, 1]$ . From (19), we can obtain  $\eta_k > 0$  can be always met. By combining the monotonically increasing property of  $g'(b_{i,k})$ , we can conclude that the root  $\eta_k^*$  of (19) is always unique and positive.  $\square$

With Proposition 2, a bisection search method can be used to obtain the optimal  $\eta_k^*$  [35], [36]. Given that  $\eta_k > 0$  always holds, we know that the equality  $\sum_{i \in \Psi_k} b_{i,k} - 1 = 0$  for  $\forall k \in \mathcal{K}$  must hold. Then, the bandwidth allocation solution can be obtained by solving equation (19) iteratively over  $\eta_k \in (0, \eta_{\max}]$ . The detailed process of the bisection search method is outlined in Algorithm 1. Given a precision  $\delta$ , Algorithm 1 requires  $O(\log_2(\frac{\eta_{\max}}{\delta}))$  number of iterations to converge.

---

**Algorithm 1** Bandwidth Allocation Solution: Bisection Search Method

---

- 1: For each group  $k \in \mathcal{K}$ , initialize  $\eta_{k,l} = 0$ ,  $\eta_{k,h} = \eta_{\max}$ ,  $\delta > 0$ , and set  $q = 0$ .
  - 2: **while**  $|\eta_{k,h} - \eta_{k,l}| \geq \delta$  **do**
  - 3:    $\eta_{k,q} = (\eta_{k,h} + \eta_{k,l})/2$  and  $q = q + 1$ .
  - 4:   Obtain the root  $b_{i,k}$  of the equation  $g'(b_{i,k}) + \eta_{k,q} = 0$  for each  $i \in \Psi_k$  by using a bisection numerical method.
  - 5:   **if**  $\sum_{i \in \Psi_k} b_{i,k} > 1$  **then**
  - 6:     let  $\eta_{k,l} = \eta_{k,q}$ .
  - 7:   **else**
  - 8:     let  $\eta_{k,h} = \eta_{k,q}$ .
  - 9:   **end if**
  - 10: **end while**
- 

Next, we will discuss how to solve the computing resource allocation. Observing the KKT conditions in (18), we know constraints (18b), (18d), (18f), (18h), and (18j) are related to computing resource allocation variable  $\mathbf{f}$ . To make it clear, in the following, we restate these constraints as

$$-\frac{U_{i,j}}{f_{i,j}^2} + \mu_j = 0 \quad \forall i \in \Pi_j, \forall j \in \{\mathcal{J} \setminus CAV\} \quad (21a)$$

$$\mu_j \left( \sum_{i \in \Pi_j} f_{i,j} - 1 \right) = 0 \quad \forall j \in \{\mathcal{J} \setminus CAV\} \quad (21b)$$

$$\sum_{i \in \Pi_j} f_{i,j} - 1 \leq 0 \quad \forall j \in \{\mathcal{J} \setminus CAV\} \quad (21c)$$

$$f_{i,j} > 0 \quad \forall i \in \Pi_j, \forall j \in \{\mathcal{J} \setminus CAV\} \quad (21d)$$

$$\mu_j \geq 0 \quad \forall j \in \{\mathcal{J} \setminus CAV\}. \quad (21e)$$

From (21a), we can conclude that

$$\frac{U_{i,j}}{f_{i,j}^2} = \mu_j, \quad \forall i \in \Pi_j, \forall j \in \{\mathcal{J} \setminus CAV\}. \quad (22)$$

Accordingly, we know that  $\mu_j > 0$  always holds (Note that both  $U_{i,j}$  and  $f_{i,j} > 0$  for  $\forall i \in \Pi_j$ ).

As a result, the following expression must hold:

$$\sum_{i \in \Pi_j} f_{i,j} - 1 = 0 \quad \forall j \in \{\mathcal{J} \setminus CAV\}. \quad (23)$$

From (22), we can obtain the following formula:

$$f_{i,j} = \sqrt{\frac{U_{i,j}}{\mu_j}} \quad \forall i \in \Pi_j, \forall j \in \{\mathcal{J} \setminus CAV\}. \quad (24)$$

Substituting (24) into (23), we can know that

$$\frac{1}{\sqrt{\mu_j}} \left( \sum_{i \in \Pi_j} \sqrt{U_{i,j}} \right) = 1 \quad \forall j \in \{\mathcal{J} \setminus CAV\}. \quad (25)$$

Therefore, we can obtain the closed-form optimal solution for the computing resource allocation as follows:

$$f_{i,j} = \frac{\sqrt{U_{i,j}}}{\sum_{i \in \Pi_j} \sqrt{U_{i,j}}} \quad \forall i \in \Pi_j, \forall j \in \{\mathcal{J} \setminus CAV\}. \quad (26)$$

The closed-form solution indicates that for CAV  $i$  in group  $j$  ( $j \neq CAV$ ), the optimal computing resource  $f_{i,j}$  is determined by the fraction of the square root of its own computation parameter  $U_{i,j}$  and the summation of square roots of CAVs' computation parameters in group  $j$ , i.e.,  $\sum_{i \in \Pi_j} \sqrt{U_{i,j}}$ .

## V. SIMULATION RESULTS

In this section, we present the simulation results to evaluate the performance of our proposed scheme. We consider a 400 m one-way road covered by two RSUs and one HAPS. The HAPS hovered in the air at an altitude of 20 km and over the middle of the road horizontally. Two RSUs were deployed at the positions of 100 m and 300 m, each of which covers a range of 200 m. In this system, ten CAVs were initially randomly deployed on the road and their speed was set as 10 m/s. There are  $N = 80$  fundamental data in the HAPS library, whose data amounts were set as 1 Mbits, 3 Mbits, and 5 Mbits randomly. We assumed that the contents in the library were sorted on the basis of their popularity. The content popularity distribution was modeled as a Zipf distribution, i.e., the probability of the requesting for the  $n$ -th content was  $\frac{n^{-\rho}}{\sum_{n=1}^N n^{-\rho}}$ , and the shape factor  $\rho$  was 0.5. Each CAV randomly generated one task to be computed which depends on the individual input data per time slot and requested the corresponding fundamental data. If not emphasized, the main parameters of tasks were randomly set as follows. The individual data amount was set as 100 Kbits, 300 Kbits, and 500 Kbits, the computation density was set as 500,

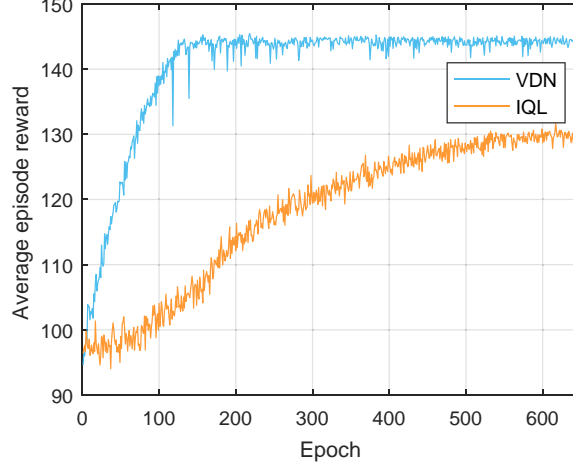


Fig. 3: Convergence of VDN algorithm.

800, and 1,100 in cycle/bit, and the output data amount was set as 60 Kbits and 90 Kbits. The computational capabilities of the CAV, RSU, and HAPS were set as 2 G, 16 G, and 50 G in CPU cycle/s, respectively. The caching space of RSU was set as 200 Mbits. For communication parameters, the transmitting power of CAV, RSU, and HAPS were set as 23 dBm, 27 dBm, and 33 dBm [37], respectively, and the available bandwidths  $B_{ul,R}$ ,  $B_{ul,H}$ ,  $B_{dl,R}$ , and  $B_{dl,H}$  were set as 5 MHz, 5 MHz, 10 MHz, and 20 MHz, respectively. The noise power spectral density was -174 dBm/Hz, and the directional antenna gain for HAPS was 17 dBi [38]. For LoS links, the small-scale fading followed a Rice distribution with rician factor 10 dB, and for NLoS links, the path-loss exponent  $\alpha$  was 3.7, and the small-scale fading followed a Rayleigh distribution  $\mathcal{CN}(0, 1)$ .

Here we show the simulation settings of the multi-agent reinforcement learning and bisection search methods. The learning process of the agents in both IQL and VDN algorithms was on the basis of the DQN, including the typical techniques of experience replay, target networks, and back propagations. The agent architecture followed [33], where the inputs were processed first by a fully connected linear layer followed by a nonlinear activation function ReLU and then a GRU-cell, which is a kind of sequential RNN layer, and finally a linear layer was adopted to output the individual  $Q$  values. The agents in the IQL algorithm trained their own networks in a decentralized manner, while following the CTDE mode and principle in (9), the VDN algorithm utilized the summation of individual  $Q$  values for centralized training to optimize the

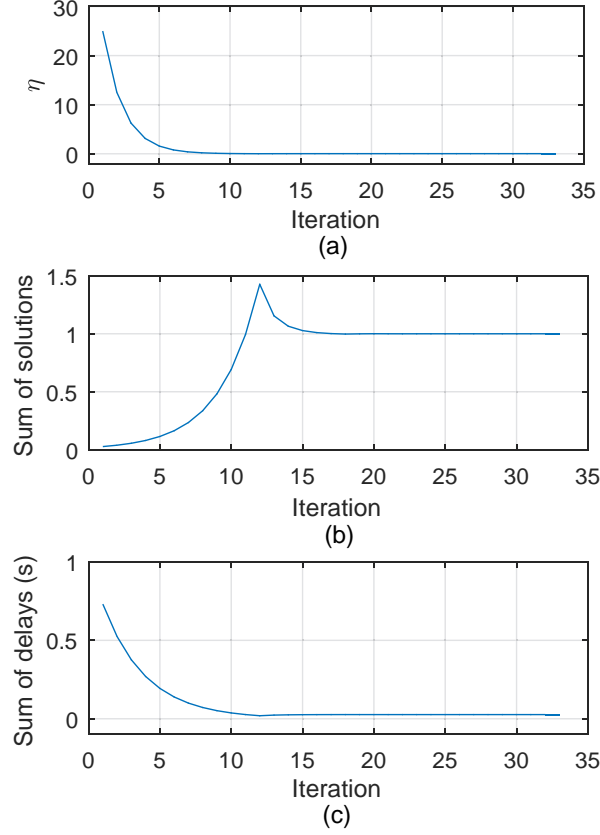


Fig. 4: Convergence and problem-solving process of Algorithm 1.

team reward. The number of units in hidden layers was set to 128. We set the learning rate and discount factor as 0.0005 and 0.95, and the minibatch and replay buffer sizes as 64 and 10,000. Moreover, the episode limitation  $T$  was 150, and each epoch consisted of eight episodes. As for the bandwidth allocation algorithm, the initializing multiplier  $\eta_{\max}$  and the convergence precision  $\delta$  were set as 50 and  $10^{-8}$ , respectively.

Fig. 3 shows the convergence performance of the VDN algorithm with the IQL algorithm as the benchmark. The evaluation is based on the average episode reward of eight episodes in each epoch. The training process of the IQL algorithm is rather unstable and slow, and it is difficult to learn a good policy. This is because all the agents train independently and can only observe the environment locally and make decisions from their local perspectives. However, the environment changes dynamically with the policy and observation of each agent. Even if each agent takes the same action based on the same local observation, the environment changes dramatically due to the various observations and actions of other agents; so it is unstable and difficult to learn,

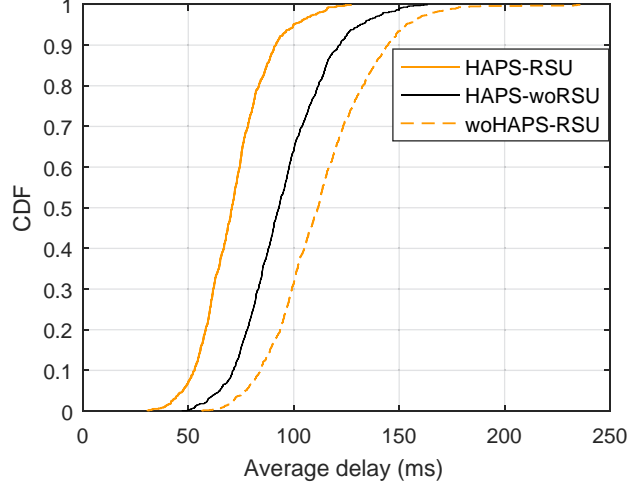


Fig. 5: CDF of average delay of CAVs over different cases.

and converges to a lower reward than the VDN algorithm. Because of its centralized training and decentralized execution (CTDE), the VDN algorithm can efficiently update the policy for each agent from a global point of view, so that each agent can learn to take action by taking into account the global situation even with local observations. Therefore, both the efficiency and stability are enhanced to some extent.

Fig. 4 shows the convergence performance and problem-solving process of the bandwidth allocation algorithm. As we can see in Fig. 4(a), the multiplier decreases rapidly as the number of iterations increases and converges around the 15th iteration. Fig. 4(b) shows the details of the summation of solutions. It is worth noting that for group  $\forall k \in \mathcal{K}$ , the KKT conditions indicate that the relationship between  $b_{i,k}$ ,  $\forall i \in \Psi_k$  and value 1 would impact the optimality of the Lagrangian function. As the iteration increases, the multiplier updates step by step, and the summation of the solutions obtained in each iteration increases with the multiplier. When the summation exceeds 1, the multiplier continues to update so that the problem-solving process is modified until the solutions converge. Fig. 4(c) shows that the objective function (summation of delays) achieves its minimization around the 15th iteration.

Fig. 5 shows the cumulative distribution function (CDF) of the average delay performance of CAVs over different cases, measured by the average of the total delay of CAVs. We let the labels ‘HAPS-RSU’, ‘HAPS-woRSU’, and ‘woHAPS-RSU’ indicate cases that there is HAPS and RSU computing, no RSU computing, and no HAPS computing, respectively. We can see

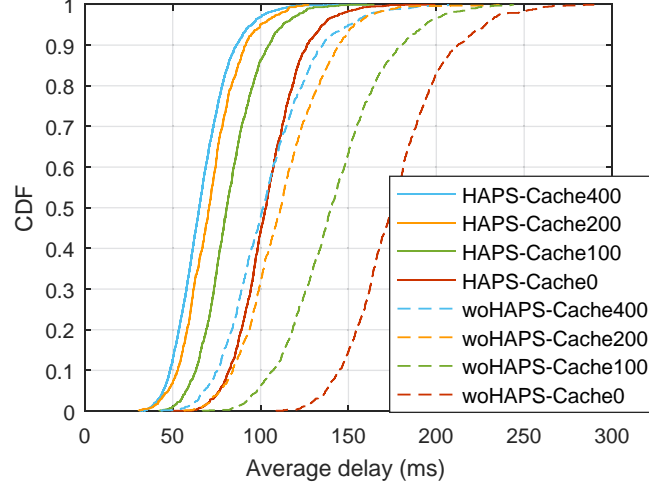


Fig. 6: CDF of average delay of CAVs vs with/without HAPS computing and caching space of RSU.

that ‘HAPS-RSU’ is the best, followed by ‘HAPS-woRSU’, and ‘woHAPS-RSU’ is the worst, which indicates that HAPS computing can mitigate delays efficiently. This happens due to two reasons: first, because of its large payload, the HAPS can be equipped with a relatively powerful computing server than RSUs, which can enhance the computational capability of the whole system. Second, HAPS computing can help to mitigate communication delays to some extent, because if some of the tasks can be computed at the HAPS, the requested fundamental data can be obtained from HAPS library directly without any transmissions. Comparing ‘HAPS-RSU’ and ‘HAPS-woRSU’, we can see the importance of RSU computing because RSUs are closer to CAVs than the HAPS. When there is no RSU computing, a large number of tasks need to be offloaded to the HAPS, which leads to large communication delays for transmitting individual input data. Accordingly, it can be reflected that HAPS computing is better to be integrated with terrestrial edge computing rather than to be replaced with it.

Fig. 6 evaluates the impact of HAPS computing and the caching space on the delay performance by comparing the CDF of the average delays. We let the labels ‘HAPS’ and ‘woHAPS’ indicate whether there is HAPS computing. The labels ‘Cache0’, ‘Cache100’, ‘Cache200’ and ‘Cache400’ indicate an RSU caching space of 0 Mbits (i.e., no caching at RSU), 100 Mbits, 200 Mbits, and 400 Mbits, respectively. As we can see, the cases with HAPS computing achieve low delays at higher probabilities than the cases without HAPS computing, which can be explained



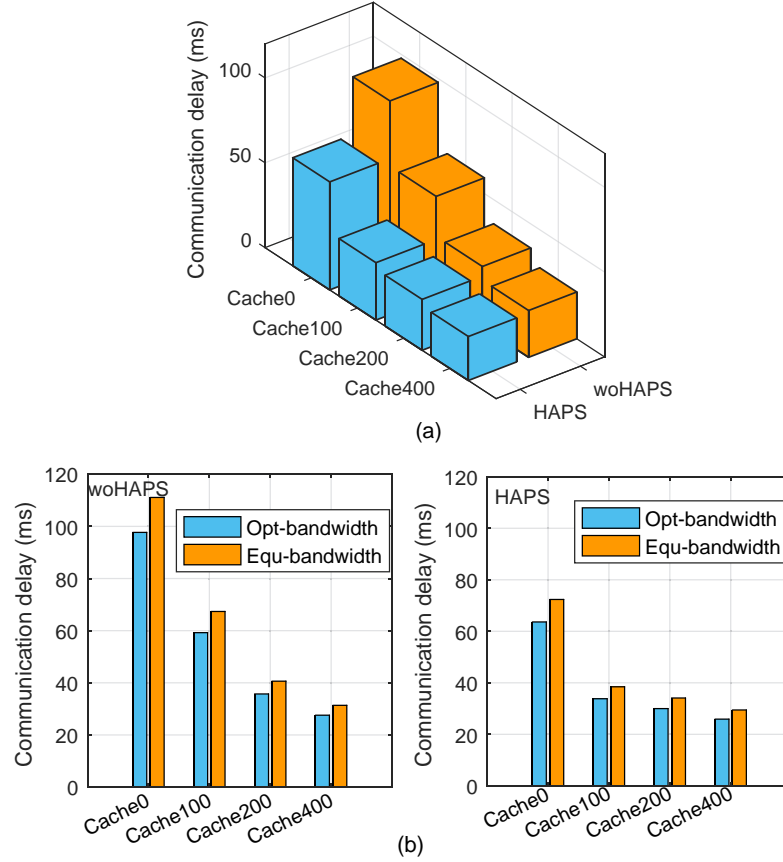


Fig. 7: (a) Communication delay vs caching space and with/without HAPS computing. (b) The comparison of the optimal bandwidth allocation and the equal bandwidth allocation.

by the same two reasons for the delay mitigation by HAPS computing as mentioned in the last paragraph. This proves the superiority of HAPS computing in combination with terrestrial networks. Also, we can see that the cases without caching are the worst, and the larger the caching space, the higher the probability of achieving low delay performance. This is because when there is no caching at RSUs, the fundamental data must be delivered from the HAPS to the ground for doing local or RSU computing, which definitely results in long-distance communication delays. By increasing the caching space, more fundamental data can be stored in advance, and therefore when doing local or RSU computing, more fundamental data can be obtained without experiencing long-distance transmission from the HAPS. To further verify the above-mentioned conclusions, we provide the communication and computation delays in Fig. 7 and Fig. 8, respectively.

Fig. 7 evaluates the communication delay performance. Fig. 7(a) shows the impact of HAPS computing and the caching space on the communication delay performance. Comparing the cases ‘Cache0’, ‘Cache100’, ‘Cache200’, and ‘Cache400’, we see that the introduction of caching at RSUs can reduce the communication delays significantly, and as more fundamental data is stored at RSUs, the communication delays can be further mitigated. Comparing the cases ‘HAPS’ and ‘woHAPS’, we can see that the introduction of HAPS computing can reduce the communication delay. Especially, the introduction of HAPS can mitigate the communication delays significantly for the case ‘Cache0’. This is because when there is no caching at RSUs, ‘woHAPS’ means that all the requested fundamental data must be transmitted from the HAPS to the ground because of the requirements of local and RSU computing; however, HAPS computing can fetch data directly from the library, so that the large communication delays caused by long-distance transmission can be avoided. Therefore, if we introduce HAPS computing in this case, the communication delays drop obviously. Fig. 7(b) shows a performance comparison of communication delays with different bandwidth allocation methods, where ‘Opt-bandwidth’ and ‘Equ-bandwidth’ indicate the optimal method and equal method for allocating bandwidth. As we can see, the optimal bandwidth allocation can effectively reduce communication delays.

Fig. 8 evaluates the computation delay performance. Fig. 8(a) shows the impact of the computational capabilities of the HAPS and RSUs on the computation delay performance. We let labels ‘HAPS0’, ‘HAPS30’, ‘HAPS50’, and ‘HAPS70’ indicate the cases where the computational capability of the HAPS is 0 G, 30 G, 50 G, and 70 G in CPU cycle/s, respectively. The labels ‘RSU10’ and ‘RSU16’ indicate the cases where the computational capabilities of RSUs are 10 G and 16 G in CPU cycle/s. Comparing ‘HAPS0’, ‘HAPS30’, ‘HAPS50’, and ‘HAPS70’, we can observe that the introduction of HAPS computing can reduce the computation delays, and by increasing the computational capability of the HAPS, the computation delays can be mitigated further since the HAPS provides more powerful computing resources to terrestrial networks. By comparing ‘RSU10’ and ‘RSU16’, two points may be observed. First, the impact of the computational capability of RSUs on computation delays is obvious, and the reason is that the RSUs are physically closer to CAVs and play an important role in computing. Second, when the computational capabilities of RSUs are lower, HAPS computing can significantly mitigate computation delays. This indicates that the introduction of HAPS computing is even more important for areas with severe resource shortages, such as remote and congested areas. In Fig. 8(b), we provide a comparison of computation delay performance for different computing

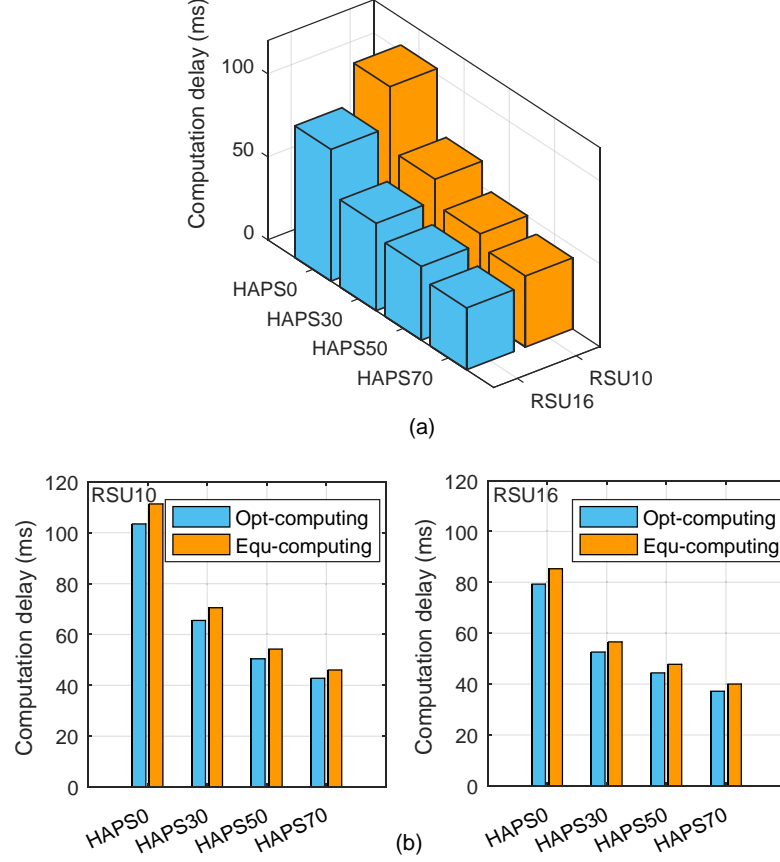


Fig. 8: (a) Computation delay vs computational capabilities of HAPS and RSU. (b) The comparison of the optimal computing resource allocation and the equal computing resource allocation.

resource allocation methods, where ‘Opt-computing’ and ‘Equ-computing’ indicate the optimal method and equal method for allocating computing resources. We can see that Fig. 8(b) verifies the superiority of the optimal computing resource allocation.

Fig. 9 shows the ratio of three computing ways: local, RSU, and HAPS computing. Fig. 9(a) shows the impact of the caching space of RSUs on the computing ratio. We can see that HAPS computing is the main computing way, especially when there is no caching, with a computing ratio of 68%. This is because when there is no caching at RSUs, more CAVs choose HAPS computing and fetch the requested fundamental data from the HAPS library directly so that the long-distance transmission of fundamental data from the HAPS can be avoided. By increasing the caching space, the ratio of HAPS computing decreases, while the ratios of local

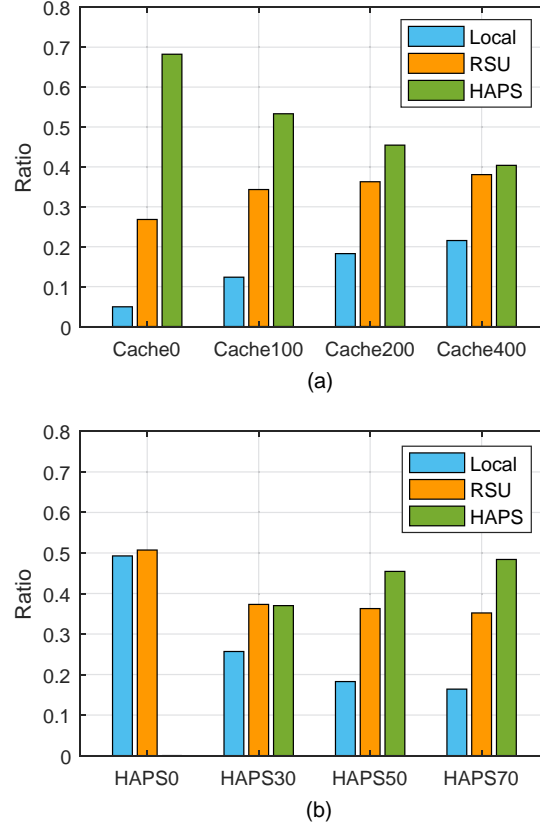


Fig. 9: (a) Computing ratio vs caching space of RSU. (b) Computing ratio vs computational capability of the HAPS.

and RSU computing increase. The reason is that as more contents can be stored at RSUs, the requested fundamental data is more likely to be obtained from the close RSUs, thereby reducing the communication delays and increasing local and RSU computing ratios. Fig. 9(b) shows the impact of the computational capability of the HAPS on the computing ratio. As the computational capability of the HAPS increases, we can see that HAPS computing ratio increases obviously, and the local computing ratio decreases. This phenomenon shows that the increase of HAPS computational capability makes HAPS computing play an increasingly important role in the system.

Fig. 10 evaluates the ratio of three computing ways for processing the tasks with different workloads. We can see that, local computing tends to process tasks with small workloads because the computational capability of each CAV is small. HAPS computing tends to process tasks with large workloads since these tasks require more powerful computational capabilities. As for RSU

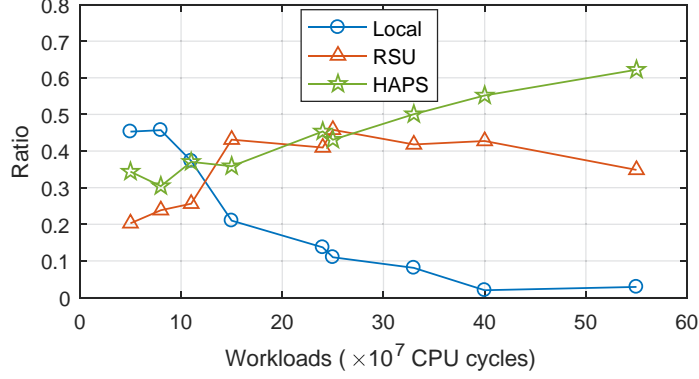


Fig. 10: Computing ratio vs workloads.

computing, it can help to process more tasks with medium and large workloads. Therefore, we know that three computing ways play different roles for processing the tasks with different workloads.

## VI. CONCLUSION

In this article, we studied a caching and computation offloading scheme with the assistance of HAPS to improve delay performance at ITS. Specifically, this scheme formulated a local-RSU-HAPS computation framework by integrating the HAPS with terrestrial computing networks, where the HAPS had a library of fundamental data. In addition, the caching technique was used at network edges in order to further mitigate the large propagation delays for delivering the requested fundamental data when executing ITS-based tasks. We formulated the problem as a delay optimization problem, where we first focused on optimizing the computation offloading and caching decisions and then focused on the allocations for bandwidth and computing resources. By utilizing the multi-agent reinforcement learning and Lagrangian methods, we solved the proposed problem. The simulation results demonstrated the advantages of the proposed scheme in improving delay performance.

Although the delay performance with a HAPS-assisted ITS has been investigated in this paper, energy efficiency was not investigated, which is important for the HAPS network. This will be studied in our future work.

## REFERENCES

- [1] S. Grigorescu, B. Trasnea, T. Cocias, and G. Macesanu, "A survey of deep learning techniques for autonomous driving," *Journal of Field Robotics*, vol. 37, pp. 362–386, Apr. 2020.
- [2] H. Zhu, K. Yuen, L. Mihaylova, and H. Leung, "Overview of environment perception for intelligent vehicles," *IEEE Transactions on Intelligent Transportation Systems*, vol. 18, pp. 2584–2601, Oct. 2017.
- [3] J. Janai, F. Güney, A. Behl, and A. Geiger, "Computer vision for autonomous vehicles: Problems, datasets and state of the art," *Foundations and Trends® in Computer Graphics and Vision*, vol. 12, pp. 1–308, Jul. 2020.
- [4] M. Chen, U. Challita, W. Saad, C. Yin, and M. Debbah, "Artificial neural networks-based machine learning for wireless networks: A tutorial," *IEEE Communications Surveys & Tutorials*, vol. 21, pp. 3039–3071, Fourthquarter 2019.
- [5] X. Yang, Z. Fei, J. Zheng, N. Zhang, and A. Anpalagan, "Joint multi-user computation offloading and data caching for hybrid mobile cloud/edge computing," *IEEE Transactions on Vehicular Technology*, vol. 68, pp. 11018–11030, Sep. 2019.
- [6] Z. Zhou, X. Chen, E. Li, L. Zeng, K. Luo, and J. Zhang, "Edge intelligence: Paving the last mile of artificial intelligence with edge computing," *Proceedings of the IEEE*, vol. 107, pp. 1738–1762, Jun. 2019.
- [7] T. Taleb, K. Samdanis, B. Mada, H. Flinck, S. Dutta, and D. Sabella, "On multi-access edge computing: A survey of the emerging 5G network edge cloud architecture and orchestration," *IEEE Communications Surveys & Tutorials*, vol. 19, pp. 1657–1681, Thirdquarter 2017.
- [8] Q. Ren, J. Chen, O. Abbasi, G. K. Kurt, H. Yanikomeroglu, and F. R. Yu, "An application-driven non-orthogonal multiple access enabled computation offloading scheme," *IEEE Internet of Things Journal*, vol. 8, pp. 1453–1466, Feb. 2021.
- [9] Y. Zhou, F. R. Yu, J. Chen, and Y. Kuo, "Cyber-physical-social systems: A state-of-the-art survey, challenges and opportunities," *IEEE Communications Surveys & Tutorials*, vol. 22, pp. 389–425, Firstquarter 2020.
- [10] Q. Luo, C. Li, T. H. Luan, and W. Shi, "Collaborative data scheduling for vehicular edge computing via deep reinforcement learning," *IEEE Internet of Things Journal*, vol. 7, pp. 9637–9650, Mar. 2020.
- [11] F. Fu, Y. Kang, Z. Zhang, F. R. Yu, and T. Wu, "Soft actor-critic DRL for live transcoding and streaming in vehicular fog-computing-enabled IoV," *IEEE Internet of Things Journal*, vol. 8, pp. 1308–1321, Feb. 2021.
- [12] X. Liu, Y. Liu, and Y. Chen, "Reinforcement learning in multiple-UAV networks: Deployment and movement design," *IEEE Transactions on Vehicular Technology*, vol. 68, pp. 8036–8049, Jun. 2019.
- [13] H. Guo and J. Liu, "UAV-enhanced intelligent offloading for internet of things at the edge," *IEEE Transactions on Industrial Informatics*, vol. 16, pp. 2737–2746, Apr. 2020.
- [14] C. Sun, W. Ni, and X. Wang, "Joint computation offloading and trajectory planning for UAV-assisted edge computing," *IEEE Transactions on Wireless Communications*, Mar. 2021. (Early Access).
- [15] S. Mao, S. He, and J. Wu, "Joint UAV position optimization and resource scheduling in space-air-ground integrated networks with mixed cloud-edge computing," *IEEE Systems Journal*, Dec. 2020. (Early Access).
- [16] N. Cheng, F. Lyu, W. Quan, C. Zhou, H. He, W. Shi, and X. Shen, "Space/aerial-assisted computing offloading for IoT applications: A learning-based approach," *IEEE Journal on Selected Areas in Communications*, vol. 37, pp. 1117–1129, Mar. 2019.
- [17] S. Yu, X. Gong, Q. Shi, X. Wang, and X. Chen, "EC-SAGINs: Edge computing-enhanced space-air-ground integrated networks for internet of vehicles," *IEEE Internet of Things Journal*, Jan. 2021. (Early Access).
- [18] J. Qiu, D. Grace, G. Ding, M. D. Zakaria, and Q. Wu, "Air-ground heterogeneous networks for 5G and beyond via integrating high and low altitude platforms," *IEEE Wireless Communications*, vol. 26, pp. 140–148, Oct. 2019.
- [19] Z. Jia, M. Sheng, J. Li, D. Zhou, and Z. Han, "Joint HAP access and LEO satellite backhaul in 6G: Matching game-based approaches," *IEEE Journal on Selected Areas in Communications*, vol. 39, pp. 1147–1159, Apr. 2021.

- [20] G. Kurt and H. Yanikomeroglu, "Communication, computing, caching, and sensing for next generation aerial delivery networks," *arXiv preprint arXiv:2011.13224*, Apr. 2021. (To appear in IEEE Vehicular Technology Magazine).
- [21] ITU, "Radio regulations articles." <http://www.itu.int/pub/R-REG-RR-2016>, 2016.
- [22] G. K. Kurt, M. G. Khoshkholgh, S. Alfattani, A. Ibrahim, T. S. J. Darwish, M. S. Alam, H. Yanikomeroglu, and A. Yongacoglu, "A vision and framework for the high altitude platform station (HAPS) networks of the future," *IEEE Communications Surveys & Tutorials*, vol. 23, pp. 729–779, Secondquarter 2021.
- [23] "The promise and challenges of airborne wind energy." Accessed: May 18, 2021. [Online]. Available: <https://physicsworld.com/a/the-promise-and-challenges-of-airborne-wind-energy/>.
- [24] "HAPSMobile and APB reach basic agreement to develop storage batteries for HAPS using all polymer battery." Accessed: May 18, 2021. [Online]. Available: [https://www.hapsmobile.com/en/news/press/2020/20201224\\_01/](https://www.hapsmobile.com/en/news/press/2020/20201224_01/).
- [25] M. S. Alam, G. K. Kurt, H. Yanikomeroglu, P. Zhu, and N. D. Dao, "High altitude platform station based super macro base station constellations," *IEEE Communications Magazine*, vol. 59, pp. 103–109, Jan. 2021.
- [26] Y. Wei, F. R. Yu, M. Song, and Z. Han, "Joint optimization of caching, computing, and radio resources for fog-enabled IoT using natural actor–critic deep reinforcement learning," *IEEE Internet of Things Journal*, vol. 6, pp. 2061–2073, Apr. 2019.
- [27] C. Wang, Y. He, F. R. Yu, Q. Chen, and L. Tang, "Integration of networking, caching, and computing in wireless systems: A survey, some research issues, and challenges," *IEEE Communications Surveys & Tutorials*, vol. 20, pp. 7–38, Firstquarter 2018.
- [28] A. Ibrahim and A. S. Alfa, "Using Lagrangian relaxation for radio resource allocation in high altitude platforms," *IEEE Transactions on Wireless Communications*, vol. 14, pp. 5823–5835, Jun. 2015.
- [29] A. Alsharoa and M. S. Alouini, "Improvement of the global connectivity using integrated satellite-airborne-terrestrial networks with resource optimization," *IEEE Transactions on Wireless Communications*, vol. 19, pp. 5088–5100, Apr. 2020.
- [30] S. Karapantazis and F. Pavlidou, "Broadband communications via high-altitude platforms: A survey," *IEEE Communications Surveys Tutorials*, vol. 7, pp. 2–31, Firstquarter 2005.
- [31] L. Panait and S. Luke, "Cooperative multi-agent learning: The state of the art," *Autonomous Agents and Multi-Agent Systems*, pp. 387–434, Nov. 2005.
- [32] N. C. Luong, D. T. Hoang, S. Gong, D. Niyato, P. Wang, Y. Liang, and D. I. Kim, "Applications of deep reinforcement learning in communications and networking: A survey," *IEEE Communications Surveys & Tutorials*, vol. 21, pp. 3133–3174, Fourthquarter 2019.
- [33] P. Sunehag, G. Lever, A. Gruslys, W. M. Czarnecki, V. F. Zambaldi, M. Jaderberg, M. Lanctot, N. Sonnerat, J. Z. Leibo, K. Tuyls, and T. Graepel, "Value-decomposition networks for cooperative multi-agent learning," *arXiv preprint arXiv:1706.05296*, Aug. 2018.
- [34] S. Boyd and L. Vandenberghe, *Convex Optimization*. Cambridge University Press.
- [35] S. Bi and Y. J. Zhang, "Computation rate maximization for wireless powered mobile-edge computing with binary computation offloading," *IEEE Transactions on Wireless Communications*, vol. 17, pp. 4177–4190, Jun. 2018.
- [36] J. B. Wang, J. Zhang, C. Ding, H. Zhang, M. Lin, and J. Wang, "Joint optimization of transmission bandwidth allocation and data compression for mobile-edge computing systems," *IEEE Communications Letters*, vol. 24, pp. 2245–2249, May 2020.
- [37] S. C. Arum, D. Grace, P. D. Mitchell, and M. D. Zakaria, "Beam-pointing algorithm for contiguous high-altitude platform cell formation for extended coverage," in *IEEE Vehicular Technology Conference (VTC2019-Fall)*, pp. 1–5, 2019.



- [38] F. B. Mismar and B. L. Evans, "Partially blind handovers for mmWave new radio aided by sub-6 GHz LTE signaling," *in IEEE International Conference on Communications Workshops (ICC Workshops)*, pp. 1–5, 2018.